Contribution from the Department of Chemistry,
University of Notre Dame, Notre Dame, Indiana 46556

# Effects of Bridging Hydrogens on Metal–Metal Bonds. 2. UV Photoelectron and UV–Visible Spectra and Quantum-Chemical Calculations for $Fe_3(\mu\text{-}H)_3(CO)_9(\mu_3\text{-}CCH_3)$ and $Co_3(CO)_9(\mu_3\text{-}CCH_3)$

ROGER L. DEKOCK,*[1] KWAI SAM WONG, and THOMAS P. FEHLNER*

*Received March 9, 1982*

The valence-level photoelectron spectrum of $Fe_3(\mu\text{-}H)_3(CO)_9(\mu_3\text{-}CCH_3)$ (II) has been measured in the gas phase with He I and Ne I radiation, and the UV–visible spectrum has been measured in solution. The observed bands in the former are assigned on the basis of model compound spectra, intensity changes with photon energy, and relative band areas. Comparison of the results with similar measurements on isoelectronic $Co_3(CO)_9(\mu_3\text{-}CCH_3)$ (I) reveals significant differences associated with the presence of the bridging H atoms in II. These are described in terms of protonation of the M–M bonds in going from I to II. Molecular orbital calculations of the Fenske–Hall type on I and II corroborate both the assignment of the spectra and the differences in going from I to II. Examination of the results of Mulliken population analyses and selected orbital contour diagrams clearly demonstrates the essential localized, hydridic, and ligandlike behavior of the bridging H atoms in II. The calculations on I and II also demonstrate that the cluster bonding of $Co(CO)_3$ and $Fe(CO)_3$ fragments in these molecules is adequately represented by CH and BH fragments.

In the preceding article we described the differences between the geometrical structures of $Co_3(CO)_9(\mu_3\text{-}CCH_3)$ (I) and $Fe_3(\mu\text{-}H)_3(CO)_9(\mu_3\text{-}CCH_3)$ (II) which highlight the role of

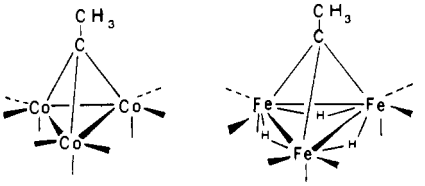


bridging H atoms in metal clusters as far as the spatial array of nuclei and core electrons are concerned.[2] We demonstrated that, in a geometrical sense, the bridging H atoms behave more like a bridging ligand than an "interstitial" atom. Here we explore the same two systems using the more sensitive tools of electronic spectroscopy and quantum chemical calculations. UV photoelectron (PE) spectroscopy[3] is the primary spectroscopic technique and provides exact, but not very detailed, information on the differences between the radical cation states of I and II. The nonparameterized Fenske–Hall molecular orbital (MO) method[4] is the quantum chemical technique of choice and provides an approximate, but detailed, view of the differences between the MO's of I and II. Although the two techniques are complementary, being related by Koopmans' theorem,[5] each provides independent information. Hence the spectroscopic comparison is developed in the first section, the overlap of spectroscopic and MO results in the second, and the MO comparison in the third. The net result is a detailed view of the role of bridging H atoms in metal clusters insofar as the distribution of valence-electron density is concerned.

## Electronic Spectra

The UV photoelectron spectra of I and II are shown in Figures 1 and 2, respectively. Before a discussion of the differences in the spectra, a qualitative assignment in terms of principal atomic character of the radical cation states is presented.[6] This assignment is derived from the spectra of model compounds, relative band areas of related ionizations, and relative band area changes with photon energy.[7] The assignment is independent of the results of calculations and, hence, independent of the validity of Koopmans' theorem.[8] Note that, as the spectrum of I has been reported by several groups already,[9-11] the assignment of this compound is outlined only briefly.

In Figure 1, the spectrum of $Co_4(CO)_{12}$, which serves as a model compound for cobalt carbonyl clusters, is also presented. This spectrum is very similar to that of $Co_2(CO)_8$[12] and consists of only two complex bands in the ionization potential (ip) region of interest. Band 1 at low ionization energy obviously contains ip's of high Co 3d character (18 ip's), and band 5 contains ip's of high CO ligand character (derived from the $5\sigma$ and $1\pi$ ip's of CO of which there are 36). The spectrum of I (Figure 1) exhibits two additional bands; namely, one at 9.76 eV (band 3) and one at about 12.6 eV (shoulder on band 5). These two bands are easily assigned to the $CCH_3$ fragment interacting with the cobalt carbonyl fragment. The assignment is summarized in Table I and is consistent with those published earlier.

The spectrum of $Fe_3(CO)_{12}$ is shown in Figure 2 and serves as a model compound for iron carbonyl clusters. Again the spectrum consists of two bands. Band 1, which now has a distinct low ip component, contains the Fe 3d ip's (12 expected), and band 5 contains the CO ligand ip's. The spectrum is not much different from that of $Co_4(CO)_{12}$ and exhibits the same open "window" from about 10 to 13 eV. The spectrum of II (Figure 2) exhibits three additional bands in this window, and by comparison with I, bands at 9.66 and 12.4 eV can be attributed to the $CCH_3$ fragment. This leaves band 4 in the spectrum of II to be assigned to the only other different component of II vs. I, i.e., the Fe–H–Fe interactions. This assignment is unambiguously confirmed by the He I (21.2 eV) and Ne I (16.8 eV) difference spectrum of bands 1–4 shown in Figure 3. Comparison of the difference spectrum with the He I spectrum shows that band 4 of II has a much larger

(1) Address: Department of Chemistry, Calvin College, Grand Rapids, MI 49506.
(2) Wong, K. S.; Haller, K. J.; Dutta, T. K.; Chipman, D.; Fehlner, T. P. *Inorg. Chem.*, companion paper in this issue.
(3) Turner, D. W.; Baker, C.; Baker, A. D.; Brundle, C. R. "Molecular Photoelectron Spectroscopy"; Wiley: New York, 1970.
(4) Hall, M. B.; Fenske, R. F. *Inorg. Chem.* **1972**, *11*, 768. Hall, M. B. Ph.D. Thesis, University of Wisconsin, Madison, WI, 1971. Fenske, R. F. *Pure Appl. Chem.* **1971**, *27*, 61.
(5) Koopmans, T. *Physica (Utrecht)* **1934**, *1*, 104.
(6) Wong, K. S.; Dutta, T. K.; Fehlner, T. P. *J. Organomet. Chem.* **1981**, *215*, C48.
(7) Rabalais, J. W. "Principles of Ultraviolet Photoelectron Spectroscopy"; Wiley-Interscience: New York, 1977.
(8) For leading references on a discussion of Koopmans' theorem see: Calabro, D. C.; Lichtenberger, D. L. *Inorg. Chem.* **1980**, *19*, 1732.
(9) Chesky, P. T.; Hall, M. B. *Inorg. Chem.* **1981**, *20*, 4419.
(10) Costa, N. C. V.; Lloyd, D. R.; Brint, P.; Spalding, T. R.; Pelin, W. K. *Surf. Sci.* **1981**, 107, L379. Costa, N. C. V.; Lloyd, D. R.; Brint, P.; Pelin, W. K.; Spalding, T. R. *J. Chem. Soc., Dalton Trans.* **1982**, 201.
(11) Granozzi, G.; Agnolin, S.; Casarin, M.; Osella, D. *J. Organomet. Chem.* **1981**, *208*, C6.
(12) Fehlner, T. P., unpublished data.

0020-1669/82/1321-3203$01.25/0 

Table I. He I Photoelectron Spectra and Calculated Eigenvalues

| $Co_3(CO)_9CCH_3$ (I) | | | | | $H_3Fe_3(CO)_9CCH_3$ (II) | | | | |
|---|---|---|---|---|---|---|---|---|---|
| band[a] | ip, eV[b] | area[c] | no. ip's; character[d] | $-\epsilon$, eV[e] | band[a] | ip, eV[b] | area[c] | no. of ip's; character[d] | $-\epsilon$, eV[e] |
| 1 | (7.45) | 12.4 | 3; Co 3d | 6.91 | 1 | (7.44) | | | |
| | 7.93 | | | 7.53 (2) | | 7.86 | 2.4 | 2; Fe 3d | 8.49 (2) |
| 2 | 8.56 | | 9; Co 3d | 8.64 | 2 | 8.63 | 7.2 | 7; Fe 3d | 9.00[f] |
| | | | | 9.13 (2) | | | | | 9.00 |
| | | | | 9.76 (2) | | | | | 9.06 (2) |
| | | | | 9.88 | | | | | 9.45 (2) |
| | | | | 10.01 (2) | | | | | 10.04 |
| | | | | 10.92 | | | | | |
| 3 | 9.76 | 3.1 | 2; Co 3d, C 2p | 12.10 (2) | 3 | 9.66 | 3.75 | 2; Fe 3d, C 2p | 11.35 (2) |
| | | | | | 4 | 11.45 | 5.5 | 3; H 1s, Fe 3d | 12.17 |
| | | | | | | | | | 12.93 (2) |
| 5 | 12.6 sh | 76.8 | ≥28; C 2p, H 1s; C 2p, O 2p | 15.6–21.1 | 5 | 12.4 sh | 76.8 | ≥28; C 2p, H 1s; C 2p, O 2p | 14.9–21.5 |
| | 14.29 | | | | | 14.36 | | | |

[a] See Figure 1 and Figure 2. [b] Vertical ip's. Adiabatic ip's are in parentheses; sh ≡ shoulder. [c] Uncorrected for instrument function. See Experimental Section. [d] Approximate major atomic orbital character of ip's. [e] Koopmans ip's from Fenske-Hall calculations; the number in parentheses refers to degeneracy. [f] The two orbitals at 9.00 eV are accidentally degenerate.

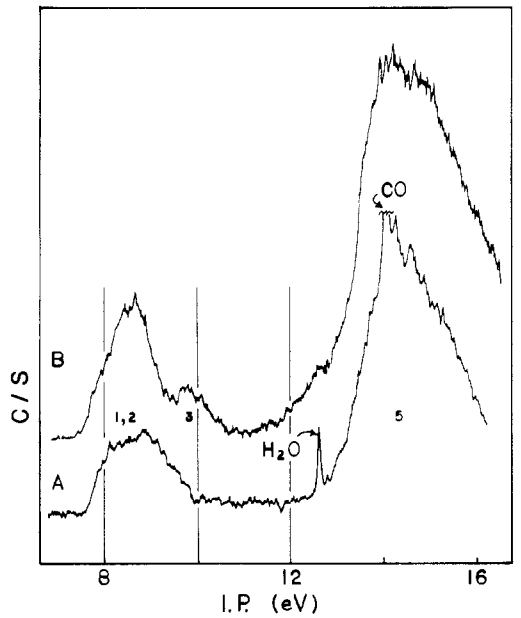


**Figure 1.** He I PE spectra of (A) $Co_4(CO)_{12}$ and (B) $Co_3(CO)_9CCH_3$.

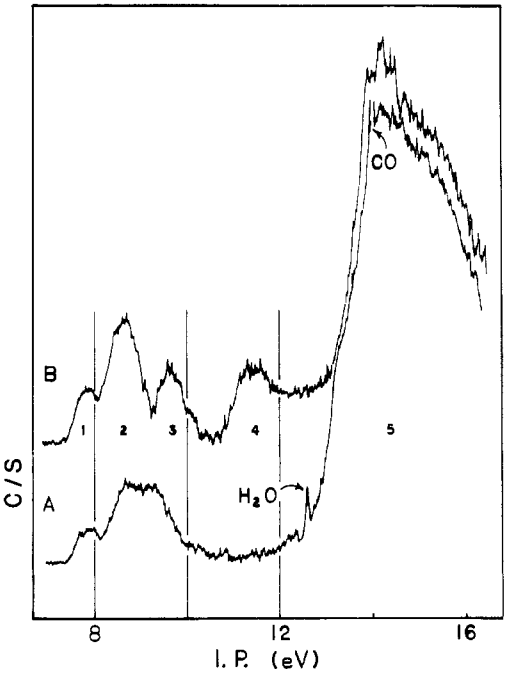


**Figure 2.** He I PE spectra of (A) $Fe_3(CO)_{12}$ and (B) $Fe_3H_3(CO)_9CCH_3$.

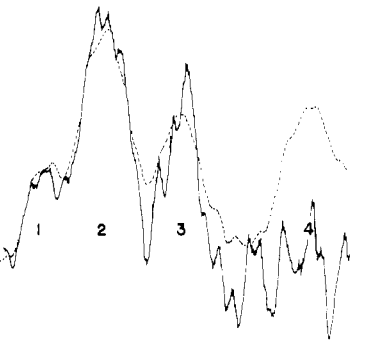


**Figure 3.** First four bands of the He I PE spectrum of $Fe_3H_3(CO)_9CCH_3$ (dotted line) and the He I minus Ne I difference with the Ne I intensity spectrum adjusted such that band 4 intensity equals zero (solid line).

relative cross section at lower photon energy than do the other bands. This is the expected behavior if band 4 possesses large H 1s character. In fact, the position of band 4 appears to be characteristic of the ionization behavior of hydrido metal carbonyls in both mononuclear and trinuclear systems.[13-15] The experimental assignments for II are given in Table I also.

A comparison of the spectra of I and II shows that the relative areas of bands 3 and 5 (Table I) are the same within experimental error. In going from I to II, however, substantial intensity is lost from bands 1 and 2, and the Fe–H–Fe band (4) appears. As three ip's are to be associated with band 4, the phenomenological explanation of this difference is that, in going from I to II, three ip's are lost from bands 1 and 2 and appear as band 4, the stabilization being about 3.5 eV. This type of difference in the spectra of isoelectronic molecules that differ only in the replacement of a nucleus of atomic number $z$ by one of $z - 1$ plus a proton has been observed in smaller systems. Comparison of the spectra of CS and HBS shows that the ip correlating with the $5\sigma$ ip of CS is stabilized 4.6 eV in going to HBS.[16] Likewise the ip that correlates with the $\pi$ ip of $C_2H_4$ is stabilized 4.2 eV in going to $B_2H_6$.[17] In

(13) Guest, M. F.; Higginson, B. R.; Lloyd, D. R.; Hillier, I. H. *J. Chem. Soc., Faraday Trans. 2* **1975**, *71*, 902.
(14) Green, J. C.; Mingos, D. M. P.; Seddon, E. A. *J. Organomet. Chem.* **1980**, *185*, C20.
(15) Green, J. C.; Mingos, D. M. P.; Seddon, E. A. *Inorg. Chem.* **1981**, *20*, 2595.
(16) Fehlner, T. P.; Turner, D. W. *J. Am. Chem. Soc.* **1973**, *95*, 7175. Kroto, H. W.; Suffolk, R. J.; Westwood, N. P. C. *Chem. Phys. Lett.* **1973**, *22*, 495.

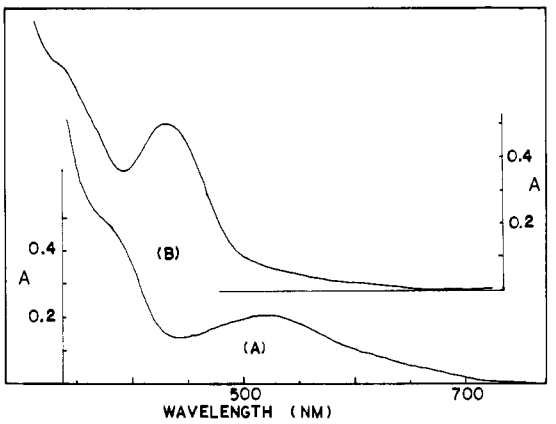


**Figure 4.** UV–visible spectra of (A) $Co_3(CO)_9CCH_3$ and (B) $Fe_3H_3(CO)_9CCH_3$.

both cases the ip in question corresponds to the removal of an electron from an orbital with a high amplitude in the region of the potential proton location. The focused stabilization by the proton far exceeds the generalized destabilization caused by the decrease in shielded nuclear charge. Hence, the three ip's lost from bands 1 and 2 in going from I to II are to be associated with 3 ip's with high localization between the metal centers, i.e., metal–metal bonding orbitals. In contrast to the view resulting from the changes in geometry caused by the bridging H atoms, here the simplest view of the changes in the photoelectron spectra are described in terms of a protonation of the metal–metal bonds in going from I to II; i.e., the bridging hydrogen acts as an interstitial proton.

As shown in Figure 4 there is also a significant difference in the UV–visible spectra of I and II. In going from I to II there is a blue shift in the lowest energy band of 80 nm (0.43 eV). With use of the simplest model, namely, that this absorption results from a one-electron transition from a high-lying filled orbital to a low-lying unfilled orbital, then the shift observed requires a stabilization of the filled orbital, destabilization of the unfilled orbital, or both. It has been demonstrated by ESR measurements on I that the lowest unoccupied molecular orbital (LUMO) is a M–M antibonding orbital of $a_2$ symmetry; i.e., there are nodes at the positions corresponding to the locations of the bridging hydrogens in II.[18] Hence, it is less likely that there will be large changes in the LUMO energy, or in fact in the other low-lying empty orbitals, in going from I to II. Via Koopmans' theorem the photoelectron spectra show that the only high-lying filled orbitals that change on going from I to II are associated with the M–M bonding. Thus, we identify the lowest energy transition in I with excitation of an electron from an orbital of M–M bonding character.

We have argued previously[6] that the comparison of the 3d bands of I and II may be used to approximately locate the position of the M–M ip's of the former. Our conclusion was that these three ip's are buried in the 3d band and that the lowest ip is not associated with a M–M bonding orbital. It is often assumed and many calculations indicate[19] that the highest occupied molecular orbital (HOMO) in systems with M–M bonds is associated with M–M bonding. Because there may well be a difference between the relaxation energies[8] of somewhat delocalized M–M bonding orbitals and localized metal "lone-pair" orbitals, the conclusions drawn from the PE

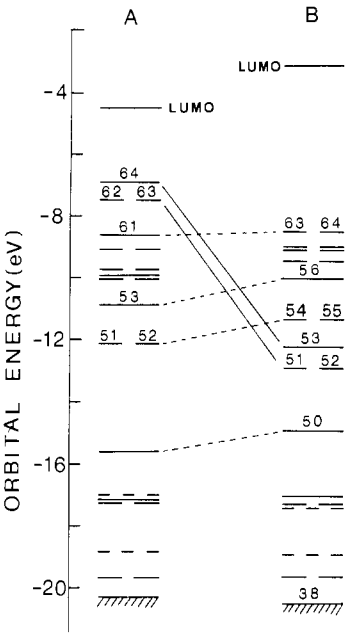


**Figure 5.** Calculated Fenske–Hall eigenvalue spectra for (A) $Co_3(CO)_9CCH_3$ and (B) $Fe_3H_3(CO)_9CCH_3$.

spectra do not eliminate the possibility that the HOMO of I is, in fact, M–M bonding. Likewise, the simplest interpretation of the lowest energy electronic excitation of I is as a transition from a M–M bonding HOMO to a M–M antibonding LUMO. On the other hand, because of differences in electronic repulsion energy[20] the lowest orbital energy difference need not correspond to the lowest energy transition. Hence, the observations on the UV–visible spectra do not require the HOMO of I to be M–M bonding. Despite the ambiguities associated with identifying state changes with orbital properties, the observations demonstrate that the comparison of the spectroscopic properties of cluster hydrides with isoelectronic clusters provides useful information on the M–M bonding in the latter.

### Electronic Spectra vs. Quantum-Chemical Calculations

The PE and UV–visible spectra presented and assigned in the previous section can be compared to molecular orbital (MO) descriptions of the molecules within the framework of Koopmans' theorem for the PE spectra and with the assumption of one-electron transitions between occupied and unoccupied MO's for the UV–visible spectra. While we keep in mind that quantitative agreement is not expected, it is the purpose of this section to examine to what extent there is agreement or disagreement between the assigned spectra and the calculated eigenvalues. A general overview of the MO description of the molecular electronic structure of I and II is followed by a comparison with the spectra.

Molecular orbital calculations were carried out on both I and II with the Fenske–Hall method. The energy level diagram for each of the two compounds is given in Figure 5, and this information is also tabulated with qualitative orbital composition designations in Table I. The isoelectronic molecules have 64 occupied MO's if we consider only the valence electrons. The first 50 MO's are predominantly associated with the CO ligands with the exception of orbitals 10, 20, 21, 26, 30, 39, 40, and 50, which are associated with the C–$CH_3$ fragment. MO 50 is mostly $M_3CC$ bonding; i.e., this orbital contains both C–C bonding and bonding of the three metal atoms to the apical carbon atom. It is not until orbital 51 that

(17) Brundle, C. R.; Robin, M. B.; Basch, H.; Pinsky, M.; Bond, A. *J. Am. Chem. Soc.* **1970**, *92*, 3863.
(18) Peake, B. M.; Robinson, B. H.; Simpson, J.; Watson, D. J. *Inorg. Chem.* **1977**, *16*, 405. Bevrich, H.; Madach, T.; Richter, F.; Vahrenkamp, H. *Angew. Chem., Int. Ed. Engl.* **1979**, *18*, 690.
(19) See, for example: Vahrenkamp, H. *Angew. Chem., Int. Ed. Engl.* **1978**, *17*, 379.
(20) See, for example: Levenson, R. A.; Gray, H. B. *J. Am. Chem. Soc.* **1975**, *97*, 6042.

a decided difference appears in comparing I and II. MO's 51–53 have no counterparts in I in that the calculated $\mu_2$-H character is almost entirely (87%) concentrated in this set of $a_1$ + e MO's.[21,22]

In a continuation in our analysis of the MO's, numbers 51 and 52 in I correlate with 54 and 55 in II, as shown in Figure 5. This pair of orbitals in both compounds consists mainly of $\pi$ bonding between the apical carbon atom and the three metal atoms in the basal plane. (The designation $\pi$ here refers to rotation around the $C_3$ symmetry axis.)

There follow nine orbitals: 53–61 for I and 56–64 for II. These are most conveniently classified as metal 3d "nonbonding", as has been done by Schilling and Hoffmann.[23] However, such a classification is only qualitatively correct. For I MO's 53–58 are about 85% Co 3d with negligible 4s and 4p contribution; MO's 59–61 are only about 50% Co 3d and 60–65% Co when the 4s and 4p contributions are included. The apical carbon $\pi$ orbitals ($2p_x$ and $2p_y$) contribute about 15% to the degenerate e MO's 59 and 60, whereas the carbon $\sigma$ orbitals (2s and $2p_z$) contribute about 7% to the $a_1$ MO 61. For II we find a roughly similar situation as with MO's 53–61 for I; i.e., the first six MO's (56–61) are 70–75% Fe 3d with little contribution from Fe 4s and 4p. The MO's 62–64 are only about 60% Fe 3d increasing to about 65% when the Fe 4s and 4p orbitals are included. The apical carbon $\sigma$ orbitals (2s and $2p_z$) contribute about 6% to the $a_1$ MO 62, whereas the $\pi$ orbitals ($2p_x$ and $2p_y$) contribute about 13% to the degenerate e MO's 63 and 64.

Finally, MO's 62–64 in I have no counterparts in II. This $a_1$ + e set of orbitals are $M_3$ bonding and constitute the "Walsh" orbitals of the $M_3$ triangle.[14] Thus, the only major difference between the eigenvalue spectra of I and II resides in MO's 62–64 in I and 51–53 in II. In both cases these orbitals serve to bind the metal triangle together, hence the solid correlation lines drawn in Figure 5. The fact that this set of three orbitals ($a_1$ + e) is substantially stabilized in going from I to II is exactly what one might have expected upon introduction of three protons to the region of M–M electron density. This sort of stabilization is also observed for one MO of $B_2H_6$ compared to $C_2H_4$[17] and other metal hydride carbonyl clusters.[15]

Note that there are some smaller differences between I and II. The nine 3d "nonbonding" MO's and the three MO's mainly involved in bonding the apical carbon to the $M_3$ triangle (50–53 for I and 50, 54, and 55 for II) are slightly (from 0.0 to 0.8 eV) less stable in II than in I. This destabilization is expected on "removing" a proton from the Co nucleus to form the Fe nucleus and is in line with the differences in the valence-orbital ionization energies of the free Co and Fe atoms.[24]

A comparative analysis of the unoccupied orbitals shows first that the LUMO is of $a_2$ symmetry and M–M antibonding for the two compounds and slightly less stable in II than in I.[25] There is no large perturbation of the LUMO in going from I to II simply because there are nodes at the bridging hydrogen positions. There is one interesting difference in the other virtual orbitals in I and II. There are three higher lying unoccupied MO's of I that are just as dramatically stabilized in going to II as the three occupied MO's (Figure 5). The orbitals that are stabilized are involved with the $M_3$ triangle and have *two* nodes between the metal atoms; i.e., they have a significant amplitude at the bridging hydrogen positions. This observation of a stabilization of unoccupied MO's due to bridging hydrogens is also evident upon a comparison of the isoelectronic $B_2H_6$ and $C_2H_4$ molecules.[26]

We turn now to the PE spectra presented in Figures 1 and 2 and compare these with the calculated energy levels in Figure 5. It is clear that the calculated energy levels are in general agreement with the empirically assigned spectra.[6] Bands 1 and 2 for both compounds are assigned to the predominantly metal MO's in both compounds; this encompasses 12 MO's (53–64) for the $Co_3$ compound and 9 MO's (56–64) for the $Fe_3$ compound. The lower intensity in bands 1 and 2 for II compared to that for bands 1 and 2 for I is clearly evident just above 8 eV, at about $^1/_2$ eV higher in energy than the leading edge of the band. Comparison of the calculated eigenvalues in Figure 5 would indicate that the "missing" intensity for the $Fe_3$ compound should be at the *onset* of the band. This indicates that the $a_1$ + e Co–Co bonding MO's (62–64) are *not* the lowest energy orbitals to ionize as predicted by the calculations within the Koopmans' theorem approximation.

The assignment of band 3 to ionization from the degenerate pair of orbitals between $M_3$ and apical carbon $\pi$ AO's is in agreement with the calculated eigenvalues (MO's 51–52 for I and 54–55 for II). Bands 1–3 are predicted by the calculations to occur at slightly lower energy in II than in I. In particular, the high-energy edge of bands 1 and 2 is predicted to shift 0.8 eV to lower energy (MO 53 of I correlating with MO 56 of II). Likewise, a 0.8-eV shift to lower energy is predicted for band 3 (MO's 51–52 of I correlating with MO's 54–55 of II). Experimentally any shift in energy of bands 1–3 between the two compounds is negligible. This lack of a predicted shift to lower energy for bands 1–3 of II may be due to a difference in relaxation energy for the two compounds, as we have discussed in our earlier communication.[6]

Band 4 in II has been assigned to the $a_1$ + e MO's involved in the Fe–H–Fe bonding, in complete agreement with the calculations. Band 5 is assigned to ionization from orbitals that are predominantly CO $5\sigma$ and $1\pi$. The calculations indicate that the leading edge of this band should be due to ionization from the $M_3C$ orbital that is cluster $\sigma$ bonding along the $C_3$ axis (MO 50). In our spectra there is evidence for such a shoulder on the leading edge of band 5, particularly for I, where there is no interference from the overlap due to band 4. Besides MO 50 and the CO $5\sigma$ and $1\pi$ orbitals, band 5 must also contain a $CH_3$-based e orbital (MO's 39–40).

We turn briefly to a discussion of the UV-visible spectra of the two compounds (Figure 4). In the simplest analysis we assign the lowest energy absorption band to a HOMO–LUMO transition. This energy gap is calculated to be 2.6 eV for I (2.4 eV observed) and 5.4 eV for II (2.8 eV observed). I is predicted to absorb light at lower energy as observed experimentally. The calculated larger energy gap for II results from both a more stable HOMO and a less stable LUMO compared to the case for the $Co_3$ compound (Figure 5).

### Valence-Electron Distributions

The advantage of the MO technique over the spectroscopic techniques used here is the detail produced on the distribution of valence electrons. The fact that both techniques are consonant in describing the differences between I and II provides justification for using some of this detail. In particular, in this section, we compare Mulliken population analyses and orbital contour diagrams for I and II.

**Charge Distribution.** A comparison of the calculated Mulliken charges for the atoms in these isoelectronic molecules

(21) This is not the situation in the model compound $CH_3CB_3H_6$,[2] where substantial H atom character is found in more than three orbitals.
(22) It is interesting to note the calculations of "surface" H atoms on large cubium clusters points to very localized interactions: van der Avoird, A.; de Graaf, H.; Berns, R. *Chem. Phys. Lett.* **1977**, *48*, 407.
(23) Schilling, B. E. R.; Hoffmann, R. *J. Am. Chem. Soc.* **1979**, *101*, 3456.
(24) Basch, H.; Viste, A.; Gray, H. B. *Theor. Chim. Acta* **1964**, *3*, 458. Ballhausen, C. J.; Gray, H. B. "Molecular Orbital Theory"; W. A. Benjamin: New York, 1964; p 122.
(25) The assignment of the LUMO to $a_2$ symmetry is in agreement with recent spectroscopic and theoretical studies.[9,18,23]
(26) Jorgensen, W. L.; Salem, L. "The Organic Chemist's Book of Orbitals"; Academic Press: New York, 1973.

**Table II.** Calculated Mulliken Atomic Charges

| $Co_3(CO)_9CCH_3$ (I) | | $H_3Fe_3(CO)_9CCH_3$ (II) | |
|---|---|---|---|
| atom | charge | atom | charge |
| Co | 0.131– | Fe | 0.311+ |
| $C_{ap}$ | 0.301– | $C_{ap}$ | 0.531– |
| $C(H_3)^a$ | 0.041– | $C(H_3)^a$ | 0.027+ |
| H | 0.004+ | H | 0.013– |
| $C_{eq}{}^b$ | 0.147+ | $\mu$-H | 0.276– |
| $O_{eq}$ | 0.048– | $C_{eq}$ | 0.081+ |
| $C_{ax}{}^c$ | 0.087+ | $O_{eq}$ | 0.034– |
| $O_{ax}$ | 0.044– | $C_{ax}$ | 0.089+ |
| | | $O_{ax}$ | 0.036– |

[a] Charge on the $CH_3$ carbon atom. [b] eq ≡ equatorial. [c] ax ≡ axial.

**Table III.** Mulliken Overlap Populations

| $Co_3(CO)_9CCH_3$ (I) | | $H_3Fe_3(CO)_9CCH_3$ (II) | |
|---|---|---|---|
| Co–Co d–d | 0.022 | Fe–Fe d–d | 0.002 |
| total | 0.111 | total | –0.008 |
| Co–$C_{ap}{}^a$ d | 0.174 | Fe–$C_{ap}$ d | 0.192 |
| total | 0.514 | total | 0.448 |
| | | Fe–($\mu$-H) d | 0.121 |
| | | total | 0.246 |

[a] $C_{ap}$ refers to the apical carbon atom.

is presented in Table II. The most noticeable comparison is that the Fe atom is 0.44 unit of charge more positive than the Co atom. That is, each Fe atom has 1.44 fewer electrons than each Co atom. The total shift of electrons from the metal atoms is then $1.44 \times 3 = 4.32$ electrons. Of this number, $1.276 \times 3 = 3.83$ electrons is transferred to the bridging H atoms. On the average 0.03 electron is transferred to each of the nine CO groups and 0.23 electron is transferred to the apical carbon atom. The $CH_3$ group retains practically the same charge in both molecules. The atom that has the largest absolute charge in each compound is the apical carbon atom with a charge of 0.30– for I and 0.53– for II. The electron-rich character of the apical carbon atom is supported by experimental evidence for I. Stable carbonium ion derivatives are known[27] (e.g., $Co_3(CO)_9CCH_2^+$), and the deformation electron density maps obtained from X-ray diffraction studies on $Co_3(CO)_9CH$ also indicate an electron-rich apical carbon atom.[28] The comparison of charge distribution for I and II is mimicked by the charge analysis on the model compounds ($CH_3CC_3H_3$ and $CH_3CB_3H_6$) that was reported in the previous paper[2] with use of the ab initio calculations. We have also carried out Fenske–Hall calculations on the model compounds at the MNDO-optimized structures and observe similar trends. Clearly the changes in going from I to II as far as a charge distribution is concerned are explained by the bonding in the main-group model compounds.

**Nature of the Bonding.** The focus of our discussion in this section will be on the bonding within the $M_3C$ cluster itself, with special attention paid to the effects that the bridging H atoms have on the cluster bonding. We will employ both Mulliken overlap population analyses and orbital contour diagrams in our discussion.

Table III lists several pertinent overlap populations for both I and II. For each overlap population involving a metal atom we have tabulated two numbers; these are for the overlap population based on the 3d orbitals only and for the total (3d, 4s, 4p). There are several points of interest. The Co–Co and Fe–Fe overlap populations are negligible compared to the value obtained between the metal atom and the apical carbon atom. The latter values are practically identical for the two compounds. A comparison of overlap populations between such disparate bonds as M–M vs. M–C should be done with caution.[29] Taken at face value, these results would appear to indicate that the tetranuclear cluster in the $Co_3$ compound is predominantly held together by the apical carbon atom strongly bonded to each of the metal atoms, an interpretation that also has been suggested by the extended Hückel calculations of Evans.[30] At the moment, we do not feel that it is prudent to draw any conclusions regarding the relative amount of M–M vs. M–C bonding in these compounds.

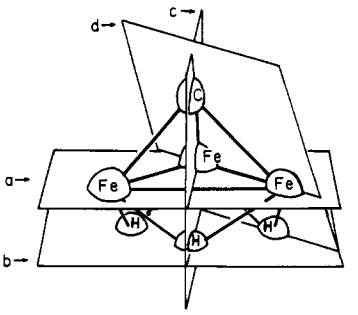


**Figure 6.** Structure of $Fe_3H_3(CO)_9CCH_3$ showing planes used to obtain orbital contours given in Figures 7 and 8.

The overlap population Fe–($\mu$-H) is substantially more than the Fe–Fe overlap population. Again, taken at face value, this would indicate that the Fe–H–Fe bond should be treated as "open" rather than "closed".[31] A similar conclusion results from a comparison of the B–B vs. B–($\mu$-H) overlap populations for the model compound $CH_3CB_3H_6$.[2] Note, however, for the model compounds, there is a much larger increase in the size of the basal atom triangle in going from $CH_3CC_3H_3$ to $CH_3CB_3H_6$. Despite this, the bonding in the main-group models is adequate to explain the changes in going from I to II.

**Molecular Orbital Contour Diagrams.** In order to enhance our understanding of the electronic structure and chemical bonding of these two isoelectronic compounds, we have drawn orbital contour diagrams for several of the orbitals in four different planes as shown in Figure 6. The four planes are labeled a, b, c, and d. Although we have made plots of numerous individual molecular orbitals, the essence of the electronic charge rearrangement can be exhibited by illustrating contours for two *sets* of molecular orbitals in each of the four planes.

The first of these two sets of orbitals is 62–64 for I and 51–53 for II (Figure 5). A comparison of the contour diagrams for these three orbitals is presented in Figure 7 for each of the four planes. In the plane of the three metal atoms (a), the orbital hybridization around the Co atom is quite different than that around the Fe atom. The $Co_3$ contours clearly exhibit the presence of overlapping 3d orbitals in the formation of Co–Co bonds. For II there is a buildup of electron density in the region between any two Fe atoms, but this clearly is not the result of overlapping 3d orbitals. Rather, it is the residual of a "sphere" of electron density surrounding the bridging H atoms. Before leaving this comparison of the plane a contours, we would also point out that the largest contour value for I is 0.05 whereas for II it is only 0.01. Clearly for

(27) For leading references, see ref 23.
(28) Leung, P.; Holladay, A.; Coppens, P. "Abstracts of Papers", 181st National Meeting of the American Chemical Society, Atlanta, GA, April 1981; American Chemical Society: Washington, D.C., 1981; INOR 90.
(29) For leading references pointing to cautions that should be observed in the interpretation of Mulliken overlap populations see: Streitwieser, A., Jr.; Berke, C. M.; Schriver, G. W.; Grier, D.; Collins, J. B. *Tetrahedron, Suppl. No. 1* **1981**, *37*, 345.
(30) Evans, J. *J. Chem. Soc., Dalton Trans.* **1980**, 1005.
(31) Bau, R.; Teller, R. G.; Kirtley, S. W.; Koetzle, T. F. *Acc. Chem. Res.* **1979**, *12*, 176.

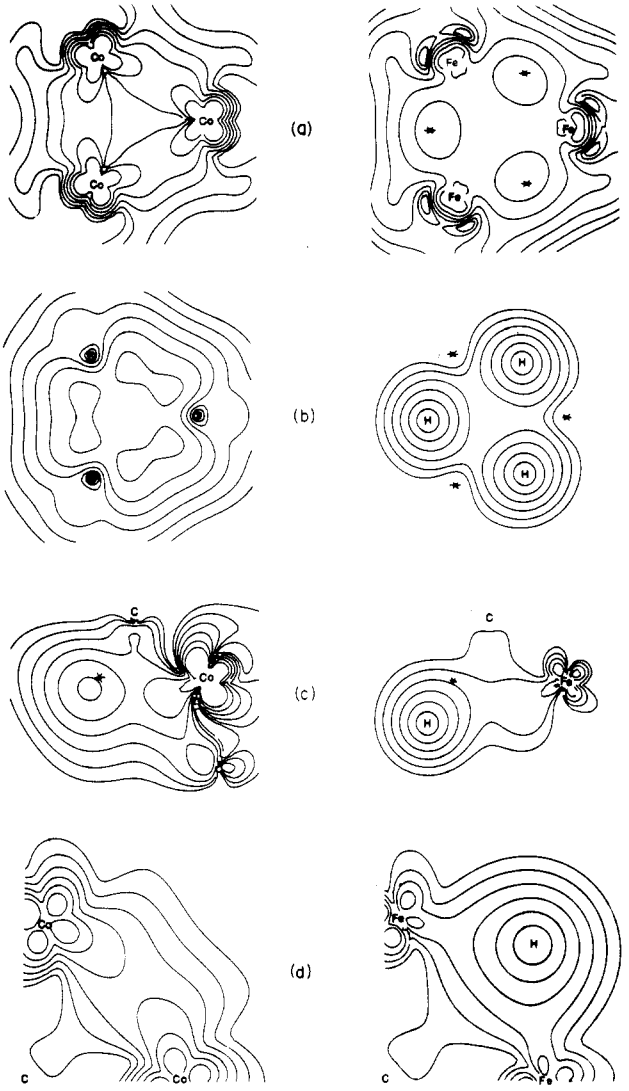


**Figure 7.** Orbital contour diagrams for MO's 62–64 of $Co_3(CO)_9CCH_3$ (left column) and MO's 51–53 of $Fe_3H_3(CO)_9CCH_3$ (right column). The contours are for planes a–d as denoted in Figure 6. The three asterisks in plane a (plane of three M atoms) denote the positions of the $\mu$-H atoms at 0.83 Å below the plane. The reverse is true for plane b. The single asterisk in plane c designates the M–M axis perpendicular to that plane. Each diagram is represented by six contours, and each succeeding contour differs from the previous one by a factor of 2.0. The values of the largest contours are as follows (units of electron $au^{-3}$): plane a, I (0.05), II (0.1); plane b, I (0.01), II (0.1); plane c, I (0.02), II (0.1); plane d, I (0.1), II (0.1).

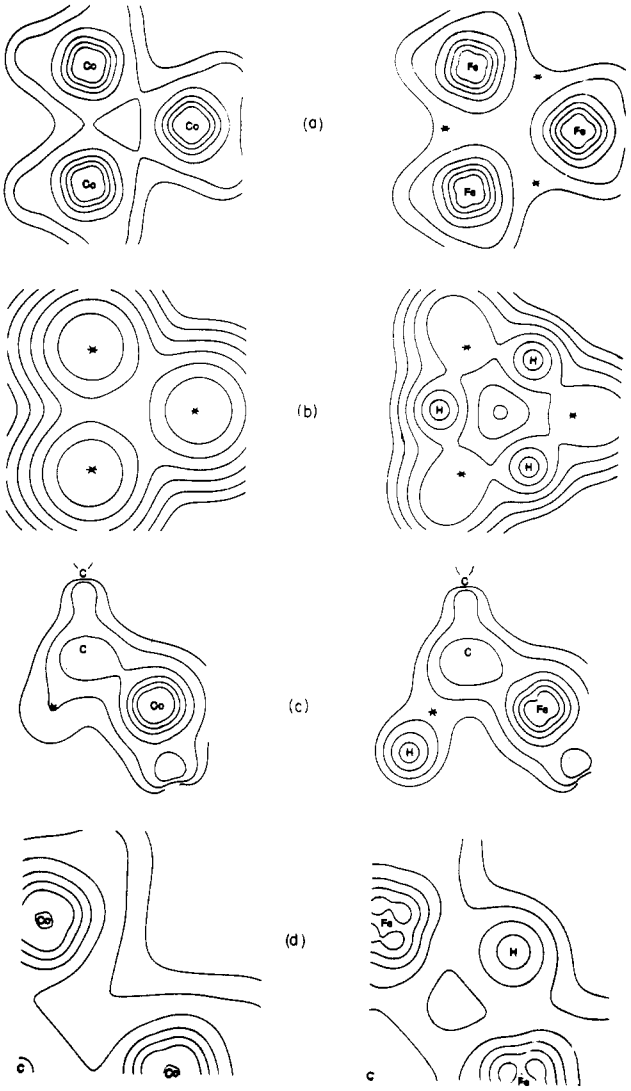


**Figure 8.** Orbital contour diagrams for MO's 41–64 of $Co_3(CO)_9CCH_3$ (left column) and of $Fe_3H_3(CO)_9CCH_3$ (right column). The same notes apply as for Figure 7. The values of the largest contours are as follows: plane a, I (0.5), II (0.5); plane b, I (0.03125), II (0.125); planes c and d, I (0.5), II (0.5).

this set of three orbitals, electron density has been shifted out of the plane of the three metal atoms and, as we shall presently see, to the plane of the bridging H atoms.

The contours in the plane of the bridging H atoms, 0.83 Å below the plane of the metal atoms, are also shown in Figure 7 for II and the analogous plane for I. In this plane, the maximum contour value for II is 0.1 and for I only 0.01. There is a large shift of electron density into the plane of the three bridging hydrogen atoms and concentrated around the three H nuclei.

The third plane that we turn our attention to is plane c of Figure 6. This plane contains the apical carbon atom, the metal atom labeled 2, and the H atom that bridges metal atoms 1 and 3 for II. Orbital contours both for this plane in II and for the corresponding plane for I are also presented in Figure 7. The contour values for II are 5 times those for I. Again, there is a substantial increase in electron density around the bridging H atoms of II. The contours for I exhibit the presence of a "bent" M–M bond. This is evident from noting the largest contour value just to the *side* of the asterisk designating the $Co_1$–$Co_3$ axis.

The fourth plane that we examine is labeled plane d in Figure 6; it contains the apical carbon atom and the two metal atoms that form one of the faces of the tetranuclear cluster. The orbital contours for plane d are also presented in Figure 7. These contours provide yet another perspective showing the buildup of electron density around the bridging H atom for II and the formation of the bent Co–Co bond for I. For plane d, the contour values in each compound have the same magnitude.

We next turn our attention to the contour diagrams containing the same four planes but encompassing the uppermost 24 occupied molecular orbitals of each compound. This set of 24 molecular orbitals includes the set of three molecular orbitals that were just examined. However, instead of focusing our attention solely on the effect of the bridging H atoms in the three MO's in which they are most concentrated, we will be able to examine features of the bonding that pertain to the cluster bonding as a whole. The latter will include effects due to the bridging H atoms, a more complete look at M–M bonding, and an examination of the bonding between the apical carbon atom and the metal atoms. The orbital contour dia-

grams for the 24 MO's (41–64) are shown in Figure 8 for all four planes and for each of the compounds.

In the plane of the three metal atoms the contours have the same value and practically the same shape. That is, in this plane the presence of the bridging H atoms seems to have had little effect on the M–M bonding in the tetranuclear cluster. For each compound the largest contour has a value of 0.5.

In the plane containing the three bridging H atoms the contour values are much less than they were in the plane of the three metal atoms, the largest values being only 0.125 for the $Fe_3$ compound and 0.03125 for I. The buildup of electron density around the bridging H atoms is still evident even in this set of 24 MO's where their relative contribution is much less than in the set of three MO's discussed previously.

In planes c and d we see the development of similar contours for both compounds between the apical carbon atom and the basal metal atom. For II there is again the buildup of electron density around the bridging hydrogen atom. The evidence for a bent Co–Co bond that was seen in the earlier contours of three MO's only is no longer evident.

Thus, it is seen that the contours for 24 of the top MO's represent more completely the nature of the cluster bonding in these molecules. For example, it is clear from these contours that there are no prominent bent Co–Co bonds, and the contours in the $M_3$ plane are practically identical in the two compounds. Furthermore, only the low-value contours "wrap around" the Fe and the $\mu$-H atoms, reinforcing the hydridic nature of the bridging hydrogen atom that was inferred from the Mulliken charge analysis.

This then brings us back to where we started. Although the changes in the PE spectra are adequately explained in terms of bridging protons buried in the M–M bonds, the detailed calculations, which reproduce the PE observations, point clearly to localized, hydridic, ligandlike bridging hydrogens. Hence, the conclusions derived from changes in geometry are consistent with those derived from an analysis of the changes in electronic structure.

## Experimental Section

**Electronic Spectra.** The samples of I and II were prepared as described elsewhere.[2,32,33] Mass spectrometric analysis of the vapor above the solid samples demonstrated that the vapor was composed of I or II. Photoelectron spectra were recorded at room temperature with the use of He I (21.2 eV and Ne I (16.8 eV) radiation. The spectrometer utilizes a 127° cylindrical-sector analyzer[3] with 10-cm radius operating at a fixed pass energy of 1.6 eV. The photoelectrons are retarded, and the retarding voltage is scanned. The spectrometer accepts photoelectrons at 90° with respect to the photon beam. The effective operating resolution, which is independent of electron energy, was 0.04 eV (fwhm). Data were accumulated on a Nicolet 1170 system with an internal calibrant of xenon and argon. The UV–visible spectra were measured on a Cary 15 spectrometer with pentane as a solvent.

**Calculations.** Fenske–Hall calculations[4] were completed on the two trimetal clusters and the model compounds $B_3H_6CCH_3$ and $C_3H_3CCH_3$. The geometries of the trimetal clusters were taken from the X-ray structural studies[2,34] but idealized to $C_{3v}$ symmetry. All C–O bond lengths were set at 1.13 Å and M–CO bond lengths at 1.80 Å. The geometries of the model compounds were taken from our calculated MNDO[35] optimized structures; these results are close to the ab initio optimized geometries.[2]

The Fenske–Hall calculations employed single-$\zeta$ Slater basis functions for the 1s and 2s functions of B, C, and O. The exponents were obtained by curve fitting the double-$\zeta$ functions of Clementi[36] while maintaining orthogonal functions; the double-$\zeta$ functions were used directly for the 2p orbitals. For hydrogen, an exponent of 1.16 was used, which corresponds to the minimum energy exponent for methane.[37] The iron and cobalt 1s–3d functions were taken from the results of Richardson et al.[38] and were all single-$\zeta$ except the 3d function, which is double-$\zeta$ and was chosen for the +1 oxidation state. Both the 4s and the 4p exponents were chosen to be 2.0. For all of the atoms studied here, these are the basis functions typically employed by Fenske and Hall in their studies using this quantum-chemical approach.

**Acknowledgment.** The support of the National Science Foundation (Grant No. CHE79-15220) is gratefully acknowledged. We thank the University of Notre Dame Computing Center for providing computing time.

**Registry No.** I, 13682-04-7; II, 69440-00-2; $Co_4(CO)_{12}$, 17786-31-1; $Fe_3(CO)_{12}$, 17685-52-8.

(32) Wong, K. S.; Fehlner, T. P. *J. Am. Chem. Soc.* **1981**, *103*, 966.
(33) Markby, R.; Wender, I.; Friedel, R. A.; Cotton, F. A.; Sternberg, H. W. *J. Am. Chem. Soc.* **1958**, *80*, 6529.
(34) Sutton, P. W.; Dahl, L. F. *J. Am. Chem. Soc.* **1967**, *89*, 261.
(35) Dewar, M. J. S.; Thiel, W. *J. Am. Chem. Soc.* **1977**, *99*, 4899.
(36) Clementi, E. *J. Chem. Phys.* **1964**, *40*, 1944.
(37) Hehre, W. J.; Stewart, R. F.; Pople, J. A. *J. Chem. Phys.* **1969**, *51*, 2657.
(38) Richardson, J. W.; Nieuwpoort, W. C.; Powell, R. R.; Edgell, W. F. *J. Chem. Phys.* **1962**, *36*, 1057.